A Family of Oxamido-Bridged $Mn^{II}Cu^{II}$ Bimetallic Molecular-Based Ferrimagnets: Synthesis, EXAFS Structural Characterization, and Magnetic Properties

Rafael Ruiz, Céline Surville-Barland, Yves Journaux,* and Jean Christophe Colin

Laboratoire de Chimie Inorganique, CNRS URA No. 420, Université de Paris-Sud, 91405 Orsay, France

Isabel Castro, Beatriz Cervera, Miguel Julve, Francesc LLoret,* and Fernando Sapiña†

Departament de Química Inorgànica, Facultat de Química, Universitat de València, Dr. Moliner 50, 46100 Burjassot, València, Spain

Received May 23, 1996. Revised Manuscript Received August 27, 1996⊗

A family of related compounds of general formula $(PPh_4)_2Mn_2[Cu(L)]_3 \cdot nH_2O$ have been synthesized, where PPh_4^+ is the tetraphenylphosphonium cation and L stands for *o*-phenylenebis(*N*′-benzyloxamidate) ($PhMe_2$opbox) (**1**), *o*-phenylenebis[*N*′-(3-phenylpropyl)-oxamidate] ($PhPr_2$opbox) (**2**), and *o*-phenylenebis[*N*′-(4-phenylbutyl)oxamidate] ($PhBu_2$opbox) (**3**). The analysis of the XANES and EXAFS spectra of **3** at both Mn and Cu K-edges reveals the occurrence of an oxamidato-bridged $Mn^{II}Cu^{II}$ two- or three-dimensional structure with Mn···Cu separation of 5.4 Å. Each manganese atom is surrounded by three Cu(L) bisbidentate entities which define an octahedral MnO_6 environment, while each copper atom is in an essentially square-planar CuN_4 surrounding. The magnetic properties of the three compounds have been investigated in the 1.8−300 K temperature range. Compounds **1**−**3** show characteristic ferrimagnetic behavior with a minimum in the χT versus T plot, and abrupt ferromagnetic phase transition below a critical temperature T_c equal to 12.5, 11.5, and 13.5 K for **1**−**3**, respectively. The magnetization versus magnetic field curve for **3** indicates that in the magnetically ordered phase, all the manganese local spins are aligned along one direction and the copper local spins along the opposite one, confirming thus the antiferromagnetic nature of the interaction between manganese(II) and copper(II) ions through the oxamidato bridge.

Introduction

The search for molecular-based magnets, i.e., compounds exhibiting a spontaneous magnetization below a critical temperature (T_c), has been a field of increasing activity in the past few years.[1] After the pioneering and exhaustive work carried out on one-dimensional compounds,[2−5] the preparation of two-dimensional ones in order to shift T_c toward higher temperatures has attracted the attention of the researchers active in this field.[6−10] However, the critical temperature, even for a chemically linked two-dimensional system remains low due to the fact that whatever the magnitude of the intraplane interaction is, the interplane interactions are very weak. Indeed, the magnetic ordering is most generally a three-dimensional phenomenon. So, the actual efforts of the chemists are directed to the design of three-dimensional networks, hoping that T_c would be very high, perhaps close to the ambient temperature.[11−14]

We report here on the synthesis and structural and magnetic characterization of a new family of ferrimagnets of general formula $(PPh_4)_2Mn_2[Cu(L)]_3 \cdot xH_2O$, where PPh_4^+ is the tetraphenylphosphonium cation and L stands for *o*-phenylenebis(*N*′-benzyloxamidate) ($PhMe_2$-opbox, **1**), *o*-phenylenebis[*N*′-(3-phenylpropyl)oxamidate] ($PhPr_2$opbox, **2**), and *o*-phenylenebis[*N*′-(4-phenylbutyl)-oxamidate] ($PhBu_2$opbox, **3**, Chart 1). The relationship between the structure and magnetic properties and the influence of the steric effects on the dimensionality, *n*D ($n = 2, 3$), are analyzed and discussed.

† Permanent address: Institut de Ciencia dels Materials, València, Spain.

⊗ Abstract published in *Advance ACS Abstracts,* October 1, 1996.

(1) Kahn, O. Magnetism of Heterobimetallics: Towards Molecular-Based magnets. In *Advances in Inorganic Chemistry*; Academic Press: New York, 1995; Vol. 43, pp 179−259 and references therein.
(2) Miller, J. S.; Calabrese, J. C.; Rommelmann, H.; Chittipeddi, S. R.; Zhang, J. H.; Reiff, W. M.; Epstein, A. J. *J. Am. Chem. Soc.* **1987**, *109*, 769.
(3) Kahn, O.; Pei, Y.; Verdaguer, M.; Renard, J. P.; Sletten, J. *J. Am. Chem. Soc.* **1988**, *110*, 782.
(4) Nakatani, K.; Carriat, J. Y.; Journaux, Y.; Kahn, O.; LLoret, F.; Renard, J. P.; Pei, Y.; Sletten, J.; Verdaguer, M. *J. Am. Chem. Soc.* **1989**, *111*, 5739.
(5) Caneschi, A.; Gatteschi, D.; Renard, J. P.; Rey, P.; Sessoli, R. *Inorg. Chem.* **1989**, *28*, 3314.
(6) Tamaki, H.; Zhong, Z. J.; Matsumoto, N.; Kida, S.; Koikawa, M.; Achiwa, N.; Hashimoto, Y.; Okawa, H. *J. Am. Chem. Soc.* **1992**, *114*, 6974.
(7) Decurtins, S.; Schmalle, H. W.; Oswald, H. R.; Linden, A.; Ensling, J.; Gütlich, P.; Hauser, A. *Inorg. Chim. Acta* **1994**, *216*, 65.
(8) Mathoniere, C.; Nuttall, C. J.; Carling, S. C.; Day, P. *Inorg. Chem.* **1996**, *35*, 1201.
(9) Stumpf, H. O.; Pei, Y.; Kahn, O.; Sletten, J.; Renard, J. P. *J. Am. Chem. Soc.* **1993**, *115*, 6738.
(10) Stumpf, H. O.; Ouahab, L.; Pei, Y.; Grandjean, D.; Kahn, O. *Science* **1993**, *261*, 447.
(11) Mallah, T.; Thiébaut, S.; Verdaguer, M.; Veillet, P. *Science* **1993**, *262*, 1554.
(12) Ferlay, S; Mallah, T.; Ouahes, R.; Veillet, P.; Verdaguer, M. *Nature* **1995**, *378*, 701.
(13) Entley, W.; Girolami, G. S. *Science* **1995**, *268*, 397.
(14) Decurtins, S.; Schmalle, H. W.; Schneuwly, P.; Ensling, J.; Gütlich, P. *J. Am. Chem. Soc.* **1994**, *116*, 9521.

S0897-4756(96)00296-7 CCC: $14.00

Chart 1

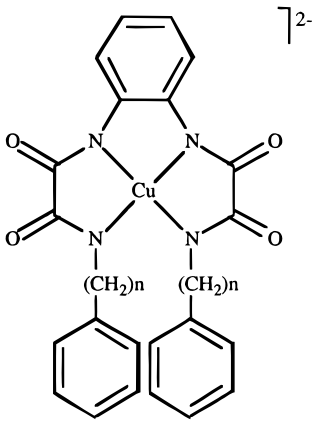

n = 1; **Cu(PhMe$_2$opbox)$^{2-}$**

n = 3; **Cu(PhPr$_2$opbox)$^{2-}$**

n = 4; **Cu(PhBu$_2$opbox)$^{2-}$**

Experimental Section

Preparation of Ligands and Mononuclear Copper(II) Precursors. The ligands *o*-phenylenebis(*N*′-benzyloxamide) (H_4PhMe$_2$opbox), *o*-phenylenebis[*N*′-(3-phenylpropyl)oxamide] (H_4PhPr$_2$opbox), and *o*-phenylenebis[*N*′-(4-phenylbutyl)oxamide] (H_4PhBu$_2$opbox) were prepared using the usual method.[15] IR ν(cm^{-1}, KBr) stretching bands: 1660, 1680sh (C═O amide) and 3295, 3350sh (N−H) for all three ligands. ^{1}H NMR data for the ligands are reported in Table S1 (supporting information).

The copper(II) tetraphenylphosphonium salts $(PPh_4)_2$[Cu(PhMe$_2$opbox)]·5H_2O, $(PPh_4)_2$[Cu(PhPr$_2$opbox])·5H_2O, and (PPh_4)-[Cu(HPhBu$_2$opbox)]·2H_2O[16] were obtained by extraction of the corresponding copper(II) tetramethylammonium salts[15] with tetraphenylphosphonium chloride in a dichloromethane/water mixture as follows: PPh_4Cl (3.75 g, 10 × 10^{-3} mol) dissolved in the minimum of water (10 mL) was added dropwise under stirring to a suspension of the corresponding tetramethylammonium salt (5 × 10^{-3} mol) in dichloromethane (100 mL). The dichloromethane phase becomes intensely colored while the aqueous phase remains colorless. After 15 min of stirring, the organic phase was separated from the mixture, washed twice with water, and dried over Na_2SO_4. The red solution was allowed to evaporate, and the resulting product was treated with acetone and ether to give a very hygroscopic red-brown solid which was rapidly collected by filtration and dried under vacuum. IR ν(cm^{-1}, KBr) stretching bands: 1565, 1605sh (C═O amide) for all complexes.

Synthesis of the Bimetallic Mn^{II}−Cu^{II} Compounds 1−3. The compounds $(PPh_4)_2Mn_2$[Cu(PhMe$_2$opba)]$_3$·10H_2O (**1**), $(PPh_4)_2Mn_2$[Cu(PhPr$_2$opba)]$_3$·10H_2O (**2**), and $(PPh_4)_2Mn_2$[Cu-(PhBu$_2$opba)]$_3$·4H_2O (**3**) were prepared as follows: Mn(CH$_3$-COO)$_2$·4H_2O (0.5 × 10^{-3} mol) dissolved in the minimum amount of dimethyl sulfoxide (DMSO) was slowly added to a solution of the tetraphenylphosphonium salt of the corresponding mononuclear copper(II) complex (1.0 × 10^{-3} mol) in DMSO (50 mL), under stirring for 15 min at 50 °C. Compounds **1**−**3** precipitate when allowing the solution to stand at room temperature. A gelatinous product is formed in the three cases which was separated by centrifugation and successively washed with DMSO, water, acetone, and diethyl ether, until it transforms in a red solid. Then it is collected by filtration and air-dried. IR ν(cm^{-1}, KBr) stretching bands: 1560, 1610sh (C═O amide).[17] Satisfactory elemental analyses were obtained for all compounds (Table S2).

Physical Techniques. ^{1}H NMR spectra were recorded at 250 MHz on a Brüker AC 250 NMR spectrometer. ^{1}H shifts are reported in δ (ppm) vs Me_4Si with the deuterated DMSO solvent proton residuals as internal standards. IR spectra were recorded on a Perkin-Elmer 882 spectrophotometer as KBr pellets. X-ray powder diffraction patterns were obtained using a Seeman-Bolhin Camera. Elemental analyses (C, H, N, Mn, Cu) were performed by the Microanalytical Service of I.C.S.N. (C.N.R.S.). The magnetic properties have been studied in the 1.8−300 K temperature range under different external fields. The magnetic susceptibility measurements have been carried out with a pendulum-type susceptometer in the 4.2−300 K temperature range under a magnetic field of 1 T, and with a SQUID (Metronique Ingenierie) magnetometer working below 30 K and down to 1.8 K at 100 G. Low-field susceptibility measurements (H = 1 G) were performed on an ac susceptometer in the 4.2−30 K temperature range at different frequencies. Magnetization measurements were carried out at 5.0 K with a pendulum-type susceptometer working with magnetic fields up to 1.4 T.

X-ray Absorption Data Collection and Processing. The XANES (X-ray absorption near-edge structures) and EXAFS (extended X-ray absorption fine structures) data were collected at LURE (Laboratoire d'Utilisation du Rayonnement Electromagnetique, Paris−Sud University) on the storage ring DCI with a energy of 1.85 GeV and a mean intensity of 300−200 mA. The measurements were carried out at both copper and manganese K-edges in the transmission mode on the EXAFS III spectrometer equipped with a two-crystal monochromator (Si 311, 0.5 mm entrance slit for both XANES and EXAFS). The monochromator was slightly detuned to ensure harmonics rejection. Reduced pressure air-filled ionization chambers were used to measure the flux intensity, before and after the sample. The spectra were recorded at 10 K in a helium cryostat designed for X-ray absorption spectroscopy.

The XANES spectra were recorded step by step, every 0.25 eV with 1 s accumulation time per point. The spectrum of a 5 μm copper or manganese foil was recorded just after or before an unknown XANES spectrum to check the energy calibration, thus ensuring an energy accuracy of 0.25 eV. The EXAFS spectra were recorded in the same way over 1000 eV, with 2 eV steps and 1 s accumulation time per point. The experiments were calibrated by using the 8991.1 eV peak at the top of the edge of a metallic foil of copper and verifying that the first inflection point in all spectra of copper and manganese foils were 8979 and 6539 eV, respectively. Each spectrum is the sum of several independent recordings added after individual inspection (two for XANES, four for EXAFS). Samples were well-pounded powders of homogeneous thickness and calculated weight, compressed between two X-ray-transparent windows. The thickness was computed in order to obtain an absorption jump at the edge $\Delta\mu x \approx 1$ with a total absorption above the edge less than $\Delta\mu x \approx 1.5$.

The XANES and standard EXAFS data analysis was performed with the GALAAD[18] and EXAFS pour le MAC[19]

(15) Ruiz, R.; Surville-Barland, C.; Aukauloo, A.; Anxolabehere-Mallart, E.; Journnaux, Y.; Cano, J.; Muñoz, M. C., submitted to *J. Chem. Soc., Dalton Trans.*

(16) Protonation of the ligand in the complex (PPh_4)[Cu(HPhBu$_2$-opbox)]·2H_2O is based both on the elemental analyses (Table S2, supporting information) and the infrared spectrum which shows a characteristic feature at 3250 cm^{-1} that may be atributed to O−H or N−H amide band. In fact, complexes with deprotonated amide nitrogens coordinated to metal ions may additionally bind protons at the amide oxygens as evidenced for other structural characterized metal ion complexes of ligands containing amido groups (*J. Chem. Soc., Chem. Commun.* **1970**, 367; **1996**, 59). In our case, this phenomenon will be favored by the inductive donor effect due to the presence of the long alkyl side chain which would enhance the basicity at the carbonyl oxygen site, promoting thus its protonation. To date, no structural evidence for both protonation and metal ion complexation at the amide nitrogen atom has been found in the literature.

(17) The C═O amide band in the IR spectra of **1**−**3** is slightly shifted to lower wavenumbers when compared to the corresponding monomeric precursors, i.e., from 1565 to 1560 cm^{-1}. This less double bond character in the C−O bond indicates coordination of the carbonyl oxygen atoms to a metal ion, confirming thus the presence of bridging oxamidato ligands in **1**−**3**. Moreover, it is also noteworthy the disappearence of the O−H band in the IR spectrum of **3** after substitution of a manganese ion for the hydrogen bound to the carbonyl oxygen in the corresponding monomeric complex.

(18) Noinville, V.; Michalowicz, A. GALAAD. In *Logiciels pour la Chimie;* Société Française de Chimie: Paris, 1991; pp 116−117.

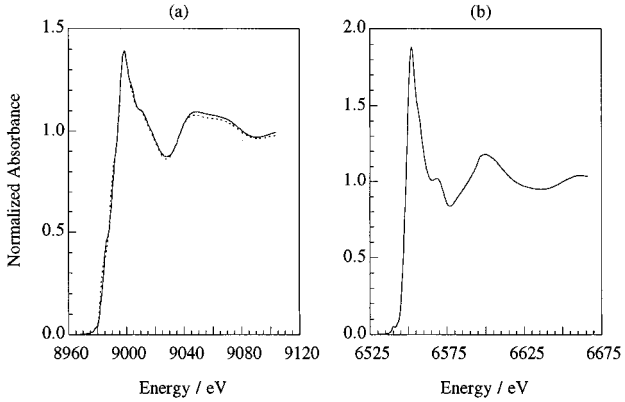

Figure 1. Normalized XANES spectra at copper (a) and manganese (b) K-edges for **3** at 10 K. The dashed line corresponds to the XANES spectrum of the related mononuclear compound $(PPh_4)_2[Cu(Me_2opbox)]\cdot 5H_2O$.

programs, and was carried out by following a well-known procedure described elsewhere.[20,21] The modeling of the outer shells is not possible in the frame of the single scattering (SS) model, and the multiple scattering/spherical-waves EXAFS ab initio modeling FEFF[22,23] program was used. Multiple scattering (MS) EXAFS contributions were included using methodology described in ref 20. The FEFF calculations were performed on a RISC system/6000 running AIX 3.2.5 of the Physical Chemistry Department of the University of Valencia.

Results and Discussion

Structural Characterization. The absence of single crystals of **1**−**3** and even their poor crystallinity do not allow us to obtain structural information by the common X-ray diffraction techniques. In fact, their powder X-ray diffraction patterns present very broad lines. Therefore, we have decided to study the XANES and EXAFS spectra of **3**, as a representative example of this family of compounds. In fact, the use of X-ray absorption techniques in this structural area is not new, and they have been previously revealed as very useful tools.[4,20]

Figure 1 displays normalized XANES spectra for compound **3** at both copper (a) and manganese (b) K-edges. The XANES spectrum of the related mononuclear compound $(PPh_4)_2[Cu(Me_2opbox)]\cdot 5H_2O$[15] ($Me_2$-opbox = *o*-phenylenebis(N′-methyloxamide)) is also shown. A comparison between the XANES spectra of **3** and $(PPh_4)_2[Cu(Me_2opbox)]\cdot 5H_2O$ at the copper K-edge reveals that the two edges are almost superimposable, suggesting strong similarities in the geometry at the metal ion (solid and dashed lines in Figure 1a, respectively). Both edges are typical of Cu(II) complexes with a very weak 1s → 3d preedge feature and an absorption edge centered on ∼8990 eV. The most important feature of the spectrum at the copper edge is that the low-energy side of the edge exhibits the characteristic shoulder of copper(II) in an elongated tetragonal surrounding.[24] The energy gap between this shoulder and the preedge is equal to 8.1 eV, a value which gives an estimate for the destabilization of the $4p_z$ metal orbital, *z* being the elongation axis. This value is close to that found in $MnCu(obbz)\cdot 5H_2O$ (obbz = oxamidobis(benzoato)), i.e., 8.6 eV.[4] It has been suggested that in elongated tetragonal copper(II) complexes, the more apart from the metal ion is the apical site, the more displaced toward the low energies is this shoulder.[24] So, in this case, the copper(II) ion appears to be in an essentially square-planar environment. The axial ligands, if any, are very far from the metal. At the manganese edge, the spectrum is typical of manganese(II) in an octahedral surrounding;[4] the intensity of the preedge is weak and the top of the edge is featureless, indicating that Mn(II) is located on a (quasi) inversion center and that the deformation of the octahedral environment is weak.[25]

The *k*-space experimental EXAFS spectra $k\chi(k)$ vs *k* at 10 K for **3**, at both copper (a) and manganese (b) K-edges, and the corresponding Fourier transforms are given in Figure 2. Manganese and copper absorption edge data were collected to $k = 15$ Å^{-1}, resulting in good resolution of peaks in the Fourier transforms. The similarity of the experimental $k\chi(k)$ values and their Fourier transforms modulus corresponding to the copper(II) monomer and **3** at copper K-edge allows us to assume that the local structure of the Cu(II) ion is almost the same for both compounds, the slight differences being attributed to the presence of the bulky substituents for compound **3**. This feature is illustrated by Figure 3. In particular, the amplitudes of the EXAFS oscillations appear unchanged. Then, there is the same number of nearest neighbors in both compounds. In fact, it is well-known that each atomic shell surrounding the metal ion is represented by a peak on the Fourier transforms. Both copper and manganese spectra for **3** comprise three main peaks. In the case of the copper K-edge (Figure 2a, bottom), the first spectrum corresponds to the four nitrogen atoms from one oxamide ligand, and the second and the third to the carbon and oxygen atoms belonging to the same oxamide ligand. At the manganese K-edge, the situation is just the inverse: the first peak corresponds to the six oxygen atoms of three oxamide ligands which belong to the coordination sphere of the metal ion, whereas the second and third peaks include essentially the six carbon and the six nitrogen atoms also from three oxamide ligands. It is particularly important to examine the two Fourier transforms upon these three main peaks: an additional weak signal is present at the manganese K-edge at a distance between 4.5 and 5.5 Å which is tentatively assigned to the intramolecular manganese−copper distances as the major contribution (see discussion below). However, the amplitude of this last peak at the copper K-edge is negligible (at the noise level) when comparing with the manganese one. The long-distance contributions can be observed only when the number of identical sites sitting at the corresponding distance from the absorbing center should not be too small and the contributing atoms should be strongly bonded or if there are important MS contributions (a linear or slightly bent three-body system is particularly amenable), which results in a weak Debye−Waller factor. These require-

(19) Michalowicz, M. EXAFS pour le MAC. In *Logiciels pour la Chimie;* Société Française de Chimie: Paris, 1991; pp 102−103.
(20) Michalowicz, A.; Moscovici, J.; Ducourant, B.; Cracco, D.; Kahn, O. *Chem. Mater.* **1995**, *7*, 1833
(21) Real, J. A.; Castro, I.; Bousseksou, A.; Verdaguer, M.; Burriel, R.; Linares, J.; Varret, F. *Inorg. Chem.*, in press.
(22) Rehr, J. J.; Zabinsky, S. I.; Albers, R. C. *Phys. Rev. Lett.* **1992**, *69*, 3397.
(23) Rehr, J. J. *Jpn. J. Appl. Phys.* **1993**, *32*, 8.
(24) Kosugi, N.; Yokoyama, T.; Asakuna, K.; Kuroda, H. *Chem. Phys.* **1984**, *91*, 249
(25) Roe, A. L.; Schneider, D. J.; Mayer, R. J.; Pyrz, J. W.; Widom, J.; Que, L., Jr. *J. Am. Chem. Soc.* **1984**, *106*, 1676

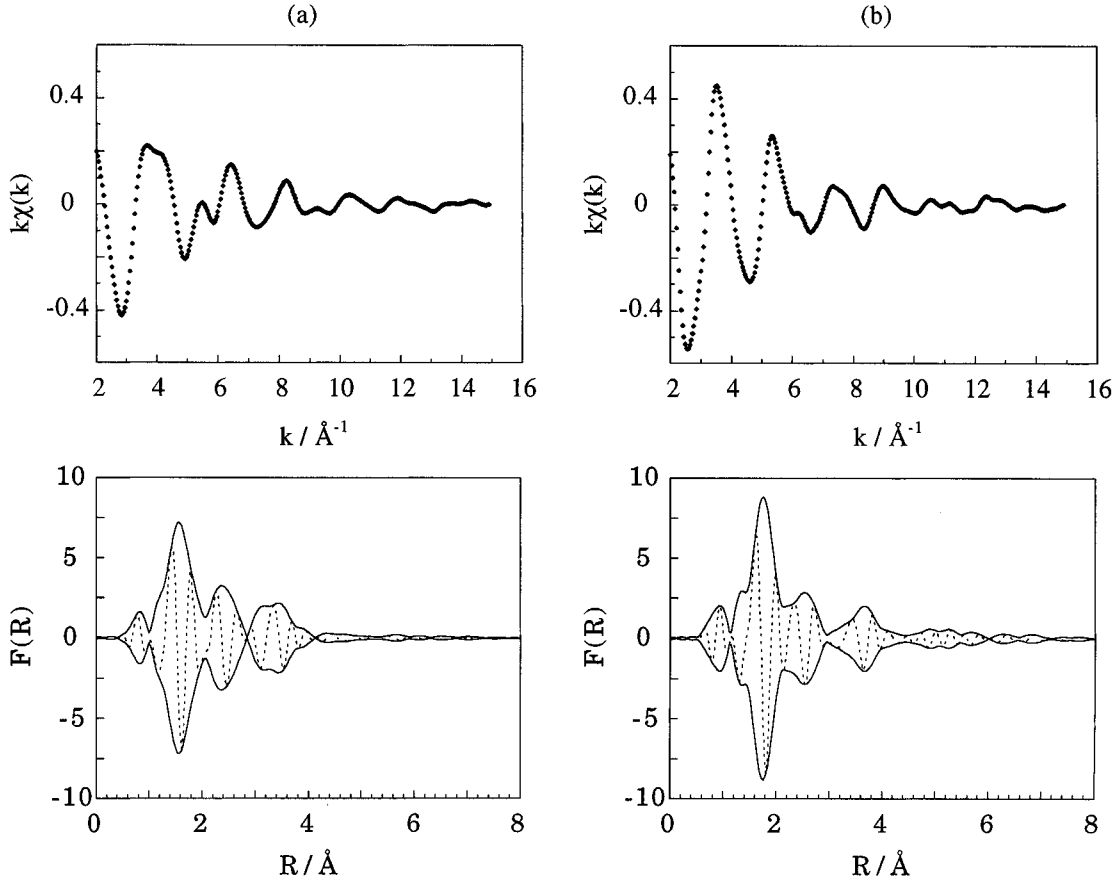

Figure 2. *k*-space experimental EXAFS spectra $k\chi(k)$ versus k (top) and Fourier transforms of the EXAFS spectra (bottom) at copper (a) and manganese (b) K-edges for **3** at 10 K.

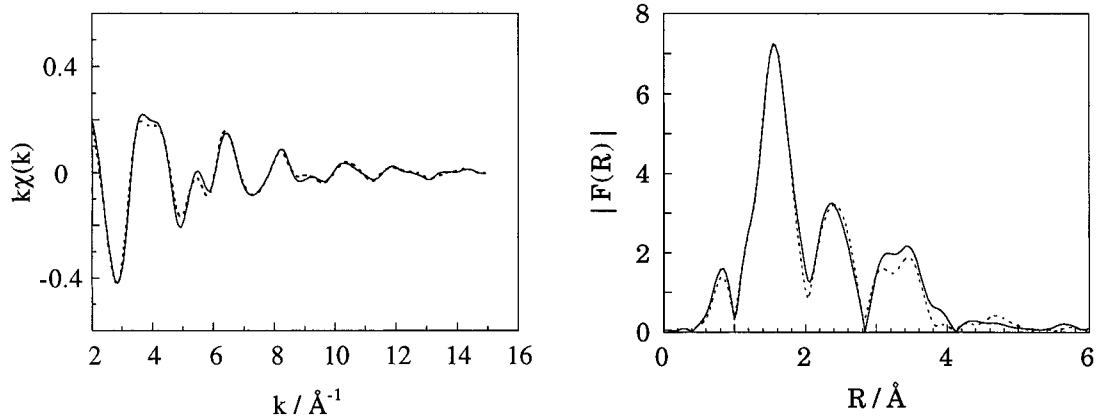

Figure 3. Comparison of the experimental $k\chi(k)$ values (left) and their Fourier transforms modulus (right) corresponding to **3** (solid line) and the related mononuclear compound $(PPh_4)_2[Cu(Me_2opbox)]\cdot 5H_2O$ (dashed line) at copper K-edge.

ments are fulfilled in the case of manganese but not in that of copper (three copper neighbors around manganese but only two manganese around copper). Moreover, there are only four MS pathways for Cu−Mn but six for Mn−Cu and much more intense, resulting in a difference of three pathways favorable for the manganese edge. The attenuation of the MS contributions in the copper(II) complexes has been interpreted as the result of dynamic disorder arising from Jahn−Teller effects;[26] thus, axial−equatorial interconversions in the copper(II) complexes will result in a large spread in outer shell distances and a consequent large increase in Debye−Waller terms for the outer shell contributions.

The number and postulated nature of neighbors, the absorber−neighbors distances, the Debye−Waller factors, and other parameters resulting from quantitative analyses of EXAFS data for the first coordination sphere of compound **3** at both manganese and copper K-edges are available in Table 1. These data confirm the above qualitative discussion. Within the frame of the single-scattering approach, the Cu(II) ion is surrounded by four nitrogen atoms with an average Cu−N(amide) bond distance of 1.97 Å and the Mn(II) ion exhibits an environment of six oxygen atoms belonging to three oxamide ligands with an average Mn−O distance of 2.18 Å. However, a complete quantitative discussion of the

(26) Fox, S.; Nanthakumar, A.; Wikström, M.; Karlin, K. D.; Blackburn, N. J. *J. Am. Chem. Soc.* **1996**, *118*, 24

(27) McKale, A. G.; Veal, B. W.; Paulikas, A. P. *J. Am. Chem. Soc.* **1988**, *110*, 3763.

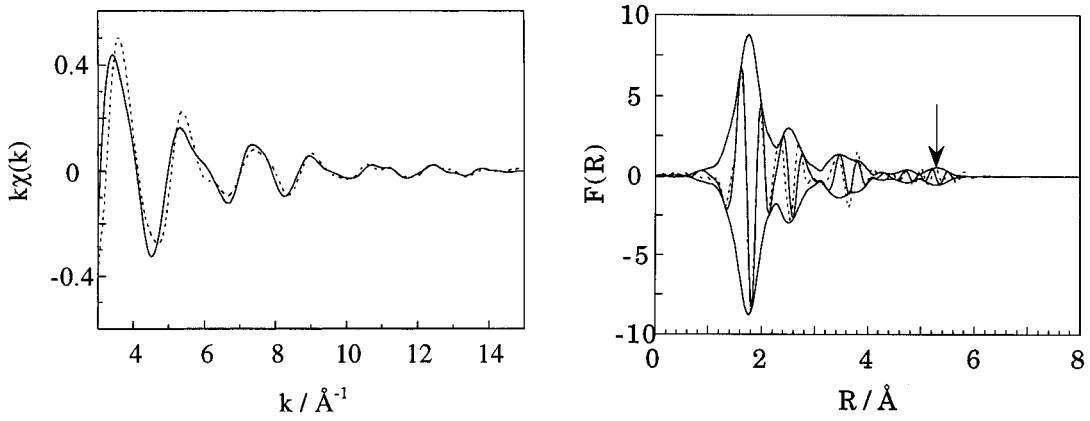

Figure 4. Comparison of the experimental (dashed line) and calculated spectrum (solid line) for **3** using the FEFF method on the model compound $(rad)_2Mn_2[Cu(opba)]_3(DMSO)_2 \cdot 2H_2O$ at the manganese K-edge: *k*-space spectra (left) and imaginary parts of the Fourier transforms for both experimental and calculated spectra along with envelope for the calculated one (right).

Table 1. Fitting of the EXAFS Data for Compound 3[a–c]

	N	*R*/Å[d]	*σ*/Å	Γ/Å	*ρ* (%)
		Cu K-Edge			
Cu-N	2	1.93(3)	0.05	0.9	0.9
	2	1.98(3)	0.05	0.9	
		Mn K-edge			
Mn−O	6	2.18(1)	0.07	0.8	2.0
Mn−C	6	2.96(3)	0.07	0.8	
Mn−N	6	4.22(4)	0.04	0.8	
Mn−Cu	3	5.43(7)	0.10	0.8	

[a] The fit at the copper K-edge was done using the experimental amplitudes and phases extracted from the mononuclear model compound $(PPh_4)_2[Cu(Me_2opbox)] \cdot 5H_2O$, whereas that at the manganese K-edge was done including the amplitude and phases extracted from FEFF calculation of the model compound $(rad)_2Mn_2[Cu(opba)]_3(DMSO)_2 \cdot 2H_2O$. [b] The results of SS fit of the first shell using the theoretical amplitudes and phases of McKale[27] are 1.95 and 1.99 Å for the Cu−N distances and 2.18 Å for the Mn−O distances, respectively, which are within the error bars. [c] *N* represents the number of atoms at the distance *R* from the copper or manganese absorber, *σ* is the Debye−Waller coefficient, Γ relates to the mean-free path of the electron and *ρ* is the least-squares fitting parameter defined as $\rho(\%) = \sum[k\chi_{exp}(k) - k\chi_{th}(k)]^2 / \sum[k\chi_{exp}(k)]^2$. [d] Errors are given in parentheses.

Scheme 1

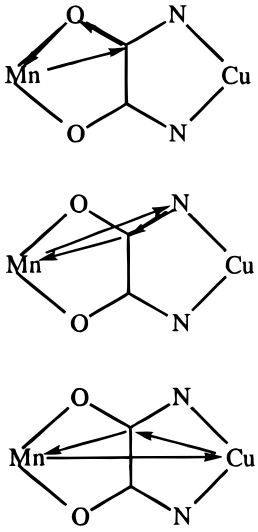

local structure around the metal ions including atoms in a sphere of 6 Å cannot be correctly performed in the frame of the single-scattering approach of the standard EXAFS formula. In fact, as illustrated in Scheme 1 for the manganese case, it can be seen that beyond the single backscattering paths (nleg = 2, nleg being the number of scattering segments in the FEFF program) many three-atom paths (nleg = 3 and 4) with scattering angles close to 180° are present. Moreover, some pathways with nleg > 4 are also significant and cannot be neglected. That being so, we have performed a FEFF calculation using $(rad)_2Mn_2[Cu(opba)]_3(DMSO)_2 \cdot 2H_2O$ [rad^+ is the organic radical cation 2-(4-*N*-methylpyridinium)-4,4,5,5-tetramethylimidazoline-1-oxyl-3-oxide and opba stands for *o*-phenylenebis(oxamate)],[28] as model compound for the environment of manganese ion in **3** (see Figure 5a). Unfortunately, this is not a good model for the case of copper, as expected. The quality of the FEFF model compared to the experimental spectrum at the manganese K-edge is illustrated in Figure 4. The imaginary part of the radial distribution functions for compound **3** is compared to the FEFF theoretical model including 262 scattering paths, calculated by FEFF on the complete set of atomic coordinates given in ref 28 (right). The large number of pathways determined by FEFF is due to the fact that the symmetry of the model compound is low and thus the degeneracy is weak. The two spectra compare quite well, in both phase and amplitude, specially at short and long distances. We have also analyzed quantitatively the first and outer shells of compound **3** at the manganese K-edge by using the amplitudes and phase shifts extracted from the FEFF calculation including the most important multiple scattering pathways (Mn−O−C, scattering angle 156°, Mn−C−N, scattering angle 175°, Mn−C−Cu, scattering angle 165° in Scheme 1). The resulting average distances are the following: six oxygen atoms at 2.18 Å (the same distance that found by simple scattering analysis, as expected), six carbon atoms at 2.96 Å, and six nitrogen atoms at 4.22 Å. These distances compare well with the crystallographic average distances in $(rad)_2Mn_2[Cu(opba)]_3(DMSO)_2 \cdot 2H_2O$ (2.18, 2.99, and 4.24 Å, respectively). Least-squares refinement resulted in the simulation shown in Figure S1 (supporting information) and the computed results are listed in Table 1. This gives an excellent fit except around $k = 5.5-6.5$ Å^{-1}. The small differences between experimental and simulated spectra in this region are due to small inaccuracies in the *k* dependence of the phases or atomic potentials for the Mn−Cu interaction as reported earlier.[26]

(28) Stumpf, H. O.; Ouahab, L.; Pei, Y.; Bergerat, P.; Kahn, O. *J. Am. Chem. Soc.* **1994**, *116*, 3866

With the use of FEFF it is now possible to come back to the peak around 5 Å in the spectrum of **3** at the manganese edge. First, since this peak will provide important information on the structure, we have tested that this peak is not due to an artifact: (i) the background was carefully analyzed by Fourier transform in order to ensure that there is no spurious signal around 5 Å in the background of the spectrum; (ii) it can be seen from the Fourier transform (Figure 2b) that this peak is clearly above the noise level; (iii) accidental fluctuations of the X-ray intensity were not observed neither in the incoming I_0 nor the transmitted beam I; (iv) the quality and homogeneity of the sample were carefully checked. As a matter of fact, the comparison of the precedent FEFF calculation and the spectrum resulting of the same model but without heavy neighbors (Figure S2, supporting information) shows that there is a peak around 5 Å in the former case but not in the latter. Therefore, we can say that the 5 Å signal (arrow in Figure 4) is not due to an experimental or mathematical artifact but arises from the location of three copper atoms around each manganese ion at a distance of 5.43 Å determined from the FEFF calculation (the mean intramolecular Cu···Mn distance in $(rad)_2Mn_2[Cu(opba)]_3(DMSO)_2{\cdot}2H_2O$ is 5.44 Å).[28]

From the complete analyses of the XANES and EXAFS data it is now possible to give a rather accurate description of the structure of compound **3**. The local structure of the manganese(II) ion in **3** should be close to that of the central manganese(II) ion in the discrete tetranuclear complex $Mn[Cu(apox)]_3(ClO_4)_2{\cdot}2H_2O$ [apox = *N*,*N*′-bis(3-aminopropyl)oxamidato] already described by us.[29] The manganese(II) ion with a octahedral geometry is coordinated to three bisbidentate copper(II) precursor units $[Cu(PhBu_2opbox)]^{2-}$, as illustrated in Figure 5a, where the large amide substituents have been schematized by an R group for clarity. Therefore, the Mn(II) coordination sphere is chiral, thus leading to two type of enantiomers, named Λ and Δ (Λ and Δ define the absolute configuration for the two possible arrangements of the copper units around the manganese atom). That is a rather important point as referred to the basic structure of this family of compounds. In fact, molecular model considerations indicate that the spatial arrangement of these chiral $[Mn(CuL)_{3/2}]$ entities can produce either a two-dimensional (2D) or a three-dimensional (3D) structure.[30] Figure 5b,c shows these 2D and 3D structures, respectively. The $[Mn(CuL)_{3/2}]$ entities are represented by octahedrons, the common edges of which symbolize the bisbidentate [CuL] planar units.

A two-dimensional honeycomb network of edge-sharing hexagons such as that schematized in Figure 5b results from the regular alternance of Λ and Δ octahedrons (each Λ octahedron is surrounded by three Δ octahedrons, and conversely). This hypothetical two-dimensional network has been recently found in the above-mentioned compound of formula $(rad)_2Mn_2[Cu(opba)]_3(DMSO)_2{\cdot}2H_2O$, confirming the perfect alternation of Λ and Δ chiral manganese centers.[28] The role of the $[PPh_4]^+$ cations in this two-dimensional model may be envisaged by considering the crystal structure of $(PPh_4)[MnCr(ox)_3]$ (ox = oxalate),[7] which belongs to the family of two-dimensional ferromagnets obtained by Okawa and co-workers of formula $(NBu_4)[MCr(ox)_3]$ (M(II) = Mn, Fe, Co, Ni, Cu).[6] In these compounds, anionic oxalate-bridged metal layers alternate with cationic ones in a regular fashion. Similarly, the role of the $[PPh_4]^+$ cations (and noncoordinated water molecules) in compounds **1**−**3** would be to separate the adjacent anionic metallic layers depicted in Figure 5b from each other.

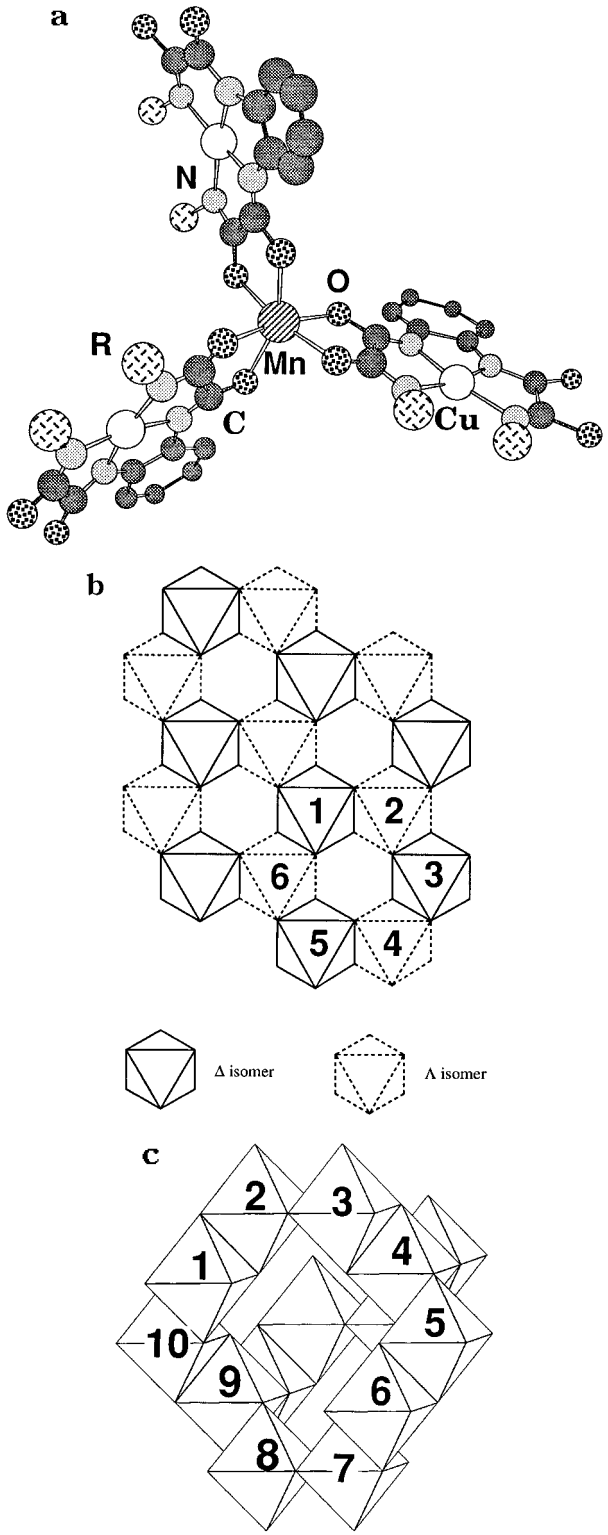

Figure 5. Postulated structures for **1**−**3**: local environment of a manganese atom (a) and schematic views of the possible two-dimensional (b) or three-dimensional (c) networks.

(29) LLoret, F.; Journaux, Y.; Julve, M. *Inorg. Chem.* **1990**, *29*, 3967.
(30) Colin, J. C. Ph.D. Thesis, University Paris-Sud, 1994.

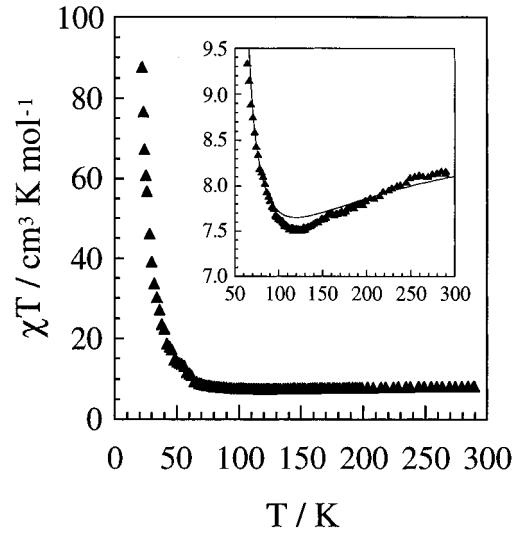

Figure 6. Experimental and calculated (solid line) χT versus T plot for **3**.

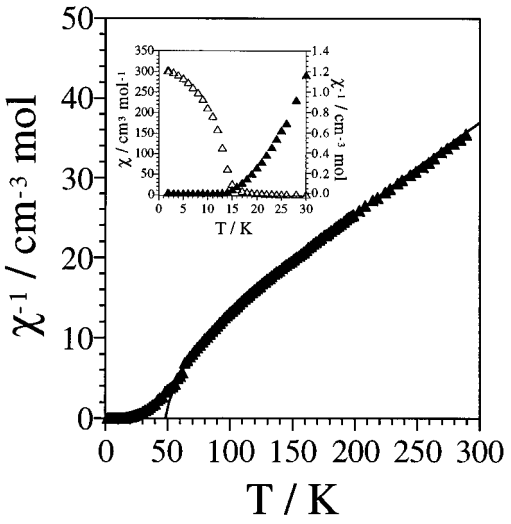

Figure 7. Experimental and calculated (solid line) $1/\chi$ and χ versus T plots for **3**.

By contrast, a three-dimensional decagon network structure is obtained when imposing the octahedrons to be only Λ or Δ. Figure 5c schematizes this three-dimensional structure made up of cycles of 10 octahedrons instead of 6 in the two-dimensional structure (Figure 5b). This hypothetical three-dimensional structure for **1**−**3** may be conceived by considering the crystal structure reported by Decurtins et al. for $[Ni(bpy)_3][Mn_2(ox)_3]$,[14] where $[Ni(bpy)_3]^{2+}$ and oxalate would replace PPh_4^+ and Cu(L), respectively. Compounds with essentially the same three-dimensional structure, of formula $[M(bpy)_3][M^{II}_2(ox)_3]$ (M^{II} = Mn, Fe) or $[M(bpy)_3][M^{I}M^{III}(ox)_3]$ (M^{I} = Li, Na, M^{III} = Cr, Fe), have also been synthesized.[14] In fact, all these compounds presents the characteristic three-connected decagon-type network illustrated in Figure 5c, along with a resolved chiral distribution of $[M(ox)_{3/2}]$ subunits as well. The trischelating $[M(bpy)_3]^{2+}$ cations with the same chirality fill the vacancies. In the case that compounds **1**−**3** were three-dimensional, the $[PPh_4]^+$ cations would fill up the large cavities within the anionic network (see Figure S3, supporting information). The size of these cavities, evaluated from EXAFS data taking as base the intramolecular Mn−Cu separation (5.4 Å), is about 30 Å (distance between two opposite manganese atoms in the cavity). This value is much greater than the mean diameter of the tetraphenylphosphonium cation. However, the presence of the bulky substituents on amide groups, which were placed within these cavities, will consequently reduce their volume down to fulfill that of the $[PPh_4]^+$ cations. Unfortunately, it is not possible to make a rational choice between one of these two basic structures (2D or 3D) for **1**−**3**, since the EXAFS data do not provide any kind of information related to the spatial distribution of the $[Mn(CuL)_{3/2}]$ units in the crystal lattice. Anyway, the subsequent study of the magnetic behavior of this family of compounds is able to bring interesting insights on this problem, as discussed below.

Magnetic Properties. The temperature dependence of the magnetic susceptibility for **3** is shown in Figure 6 in the form of the χT versus T plot, χ being the molar magnetic susceptibility per Mn_2Cu_3 unit and T the temperature. The magnetic properties of **1** and **2** are essentially similar (Figures S4 and S5, respectively, supporting information). At room temperature, χT equals 8.15 cm^3 K mol^{-1}, a value which is slightly below that expected for two Mn(II) and three Cu(II) isolated ions. χT decreases as the temperature is lowered, exhibits a rounded minimum around 120 K with χT = 7.5 cm^3 K mol^{-1} (inset of Figure 6), then increases more and more rapidly as T is lowered further, and reaches extremely high values before becoming strongly field dependent around 15 K. At 10 K, χT is as high as 2000 cm^3 K mol^{-1}. These data are characteristic of a ferrimagnetic behavior with Mn(II)−Cu(II) antiferromagnetic interactions and noncompensation of the local spins in the ground state, as is also evidenced by the $1/\chi$ versus T plot shown in Figure 7, which displays the typical hyperbolic shape of a ferrimagnetic compound. A linear plot in the range of ca. 150−300 K is observed, with a negative value of the Weiss constant $\theta = -26$ K, that confirms the antiferromagnetic nature of the interaction between Mn(II) and Cu(II) ions through the oxamidate bridge.

The temperature dependence of the magnetic susceptibility in the low-temperature region is given in the inset of Figure 7, in the form of χ and $1/\chi$ versus T plots. Upon cooling, χ shows a rapid increase with a change of sign for the second derivative $\partial^2\chi/\partial T^2$ at 13.5 K and finally becomes saturated. χ equals 300 cm^3 mol^{-1} at 1.8 K, the lowest temperature we have investigated. $1/\chi$ vanishes at 13.5 K. These data indicate that the compound behaves as a magnet with a spontaneous magnetization below 13.5 K. The temperature of ferromagnetic phase transition was determined independently by the measurement of the thermal dependence of both the in-phase, χ', and out-of-phase, χ'', components of the ac magnetic susceptibility for all three compounds as illustrated in Figure 8. The χ' curves show an abrupt break as the temperature is lowered for each compound, e.g., around 12.5 K for **1**, 11.5 K for **2**, and 13.5 K for **3**, which agrees with the appearance of an out-of-phase signal in the χ'' curves (inset of Figure 8) characteristic of a magnetic ordered state existing below this temperatures. T_c is then equal to 12.5 (**1**), 11.5 (**2**), and 13.5 K (**3**). Upon further cooling, both χ' and χ'' reach a maximum and then decrease as T is lowered, owing to the magnetic domain formation in the ferromagnetic ordered sample.

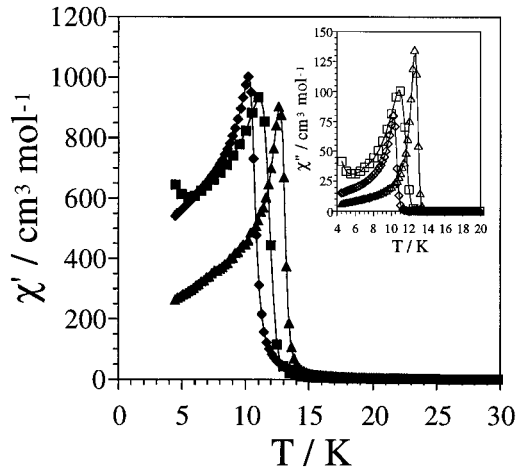

Figure 8. χ' and χ'' versus T curves for **1** (squares), **2** (rhombus), and **3** (triangles).

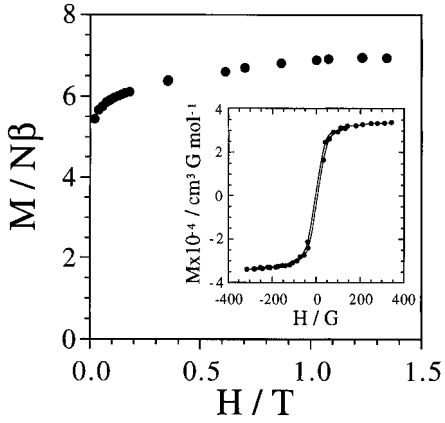

Figure 9. M versus H plot for **3** at $T = 5$ K.

Finally, the field dependence of the magnetization for **3** is shown in Figure 9 in the form of the M versus H plot, M being the molar magnetization per Mn_2Cu_3 expressed in $N\beta$ units and H the applied magnetic field. The shape of the magnetization curve at 5 K is typical of an almost ideal magnet, with around 75% of the saturation reached within a field of about 100 G. The saturation magnetization value, $M_S = 7.0\ N\beta$, nicely agrees with that calculated from equation $M_S = N\beta gS$ (S being the spin quantum number for unit formula) for the situation corresponding to the S_{Mn} local spins aligned along the field direction and the S_{Cu} local spins along the opposite direction, i.e., $S = 2S_{Mn} - 3S_{Cu}$ (with $S_{Mn} = {}^5/_2$, $S_{Cu} = {}^1/_2$, $g = 2$). The magnetic hysteresis loop at 5 K is characteristic of a soft magnet with a small coercive field of about 5 G and a low value of the remnant magnetization of 1000 cm^3 G mol^{-1} (inset of Figure 9).

At this stage, it is convenient to consider the relation between the magnetic properties and the possible structure for this family of compounds. If the assumption of three-dimensional structures for our compounds is correct (Figure 5c), the magnetic susceptibility data may be quantitatively interpreted with a two-sublattice molecular-field model (mean-field approximation)[31,32] in which the susceptibility is deduced from a spin Hamiltonian of the form

$$H_{Mn} = -zJ_{MnCu}S_{z,Mn}\langle S_{z,Cu}\rangle + g_{Mn}\beta S_{Mn}B$$

$$H_{Cu} = -z'J_{MnCu}S_{z,Cu}\langle S_{z,Mn}\rangle + g_{Cu}\beta S_{Cu}B$$

where z and z' are the number of nearest neighbors (nn) for Mn and Cu atoms respectively and $\langle S_{z,M}\rangle$ is the average value of the z component of S_M. The next-nearest neighbors (nnn) interactions between atoms of the same kind are neglected. The parameters of this model are the effective interaction parameter between adjacent spin carriers, J_{MnCu}, and the local g factors g_{Mn} and g_{Cu} for each ion, which account for the Zeeman perturbation. The least-squares fitting of the experimental data in the 60−300 K temperature range for **3** leads to $J_{MnCu} = -16\ cm^{-1}$, $g_{Mn} = 1.87$, and $g_{Cu} = 2.10$. The theoretical curve (solid line in the inset of Figure 6) is below the experimental one from ambient temperature, closely reproduces the position of the minimum around 120 K, and then passes slightly above the experimental points. The difference between theoretical and experimental curves becomes more pronounced when approaching 50 K. At that temperature, the χT values deduced from the 3D theoretical model diverge while the observed ones remain small. That strongly suggests that our compounds have not a three-dimensional network structures but two-dimensional, despite the general inadequacy of the mean-field approximation used herein. In fact, the critical temperature, T_c, which is the temperature at that a magnetization appears in the two sublattices without a magnetic field within this model might be estimated as $({}^1/_{3k})|J_{MnCu}|[zz'S_{Mn}(S_{Mn}+1)S_{Cu}(S_{Cu}+1)]^{1/2}$. By introducing the calculated J_{MnCu} value consistent with the temperature of the minimum around 120 K, and the spin quantum numbers of metal ions (with $z = 3$ and $z' = 2$ taken in this case), T_c is evaluated to be 50 K (solid line in Figure 7). In **3**, T_c is equal to 13.5 K, which indicates that our compound assumes a two-dimensional structure (Figure 5b), and the small value of the critical temperature is determined by the weak magnitude of the interplane interaction as mentioned in the Introduction. In compounds **1** and **2**, the planes consisting of edge-sharing hexagons should be slightly farther to each other due to the presence of a high number of water molecules, which results in a decrease of T_c.

Conclusions

The design and synthesis of a three-dimensional magnet represents a real supramolecular challenge as discussed by Decurtins in a very stimulating talk.[33] At this regards, it deserves to be noted that tetrahedral-shape cations (e.g., $[NBu_4]^+$ or $[PPh_4]^+$) afford two-dimensional (2D) oxalato-bridged $[M^{II}M^{III}(ox)_3]^-$ polymeric metal assemblies exhibiting magnetic phase transitions in the range 6−14 K (for M(III) = Cr, M(II) = Mn, Fe, Co, Ni, Cu)[6,7] or at even higher temperatures as, for instance, 43 K for $(NBu_4)[Fe^{II}Fe^{III}(ox)_3]$.[8] By contrast, with tris-chelated $[M(bpy)_3]^{2+}$ cations, where M is a divalent transition-metal ion and bpy is 2,2′-bipyridine, anionic three-dimensional (3D) oxalato-

(31) Herpin, A. In *Théorie du magnétisme*; Bibliothèque des Sciences et Techniques Nucléaires: Saclay, 1968; p 620.
(32) Palacio, F. In *Localized and Itinerant Molecular Magnetism*; Coronado, E., Delhaes, P., Gatteschi, D., Miller, J. S., Eds.; Kluwer: Dordrecht, 1995; p 5.
(33) Decurtins, S. In *Magnetism: A Supramolecular Function*; Kahn, O., Ed.; Kluwer: Dordrecht, 1996; p 487.

Chart 2

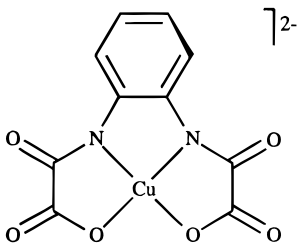

Cu(opba)$^{2-}$

bridged $[M^{II}_2(ox)_3]^{2-}$ (M^{II} = Mn, Fe) or $[M^{I}M^{III}(ox)_3]^{2-}$ (M^{I} = Li, Na; M^{III} = Cr, Fe) metal networks have been successfully achieved.[14] It has been suggested that in these systems the ideal size and symmetry of the $[M(bpy)_3]^{2+}$ cations to fill the cavities of the anionic oxalato-bridged metallic network is at the origin of the accessibility of the 3D polymeric structure with respect to the 2D one. However, despite their fascinating 3D structure, the obtention of an oxalato-bridged molecular-based magnet has not been achieved.

In this sense, the polymeric oxamato-bridged compounds of formula $(NBu_4)_2Mn_2[Cu(opba)]_3 \cdot 6DMSO \cdot H_2O$[10] and $[Ru(bpy)_3]Mn_2[Cu(opba)]_3 \cdot 13H_2O$[34] recently obtained by Kahn and co-workers, can be related to the above family of oxalato-bridged compounds by simply replacing ox^{2-} by the copper(II) precursor $[Cu(opba)]^{2-}$ (Chart 2), which relates to the class of Cu(II) monomeric complexes used herein. Surprisingly, both compounds are 2D as the parent $(rad)_2Mn_2[Cu(opba)]_3(DMSO)_2 \cdot 2H_2O$.[28] In fact, even if their crystal structures are unknown, their 3D nature can be almost discarded in the light of the low values of their critical temperatures (T_c in the range 12−25 K). The increase of the cavity size when replacing oxalato by $[Cu(opba)^2]^-$, would account for this disappointing result when compared to that obtained with the oxalato-bridged family discussed above.

In this sense, our attempts to tune the cavity size in the hypothetical 3D anionic network to accommodate the PPh_4^+ cation by substituting the $[Cu(opba)]^{2-}$ precursor by the larger $[Cu(PhMe_2opbox)]^{2-}$, $[Cu(PhPr_2opbox)]^{2-}$, and $[Cu(PhBu_2opbox)]^{2-}$ derivatives, even if it seems to be a basic prerequisite, it is not sufficient.[35] In fact, a novel family of two-dimensional oxamido-bridged bimetallic molecular-based ferrimagnets with critical temperatures around 10 K has been obtained, which adds to the existing oxamato-bridged family of Kahn's group[9,28,34] and to the oxalato- and dithiooxalato-bridged ones reported quite recently by Day[8] and Okawa,[36] respectively. Therefore, our approach to prepare a 3D molecular-based magnet by modifying the precursor size has been revealed as an excessively naive picture because it ignores the peculiar kind of interactions established between the cations and the anionic network. The fundamental role of the multiple noncovalent interactions (π-stacking between aromatic rings, hydrophobic interactions, van der Waals forces, hydrogen bonds) as the mechanistic origin of organized three-dimensional architectures is well-known in biochemistry, but unfortunately it is not as well developed in synthetic chemistry.[37] In a certain sense, the problem we are faced with when trying to obtain a 3D molecular-based magnet is reminiscent of the well-known lock-and-key biological principle formulated by Fischer to explain the enzyme-substrate interaction.[38] Up to now, we are still on the pursuit for the "key".

Acknowledgment. We thank Dr. J. Sainton for the achievement of the ^{1}H NMR spectra and Dr. T. Coradin for the realization of the X-ray powder diffractograms. We would also like to express our gratitude to Dr. F. Villain for the help in the use of the EXAFS 3 spectrometer and cryogen device and Prof. Michalowicz from the LURE for his help in the use of the FEFF program and fruitful discussions. Financial support from the Dirección General de Investigación Científica y Técnica (DGICYT, Spain) through Project PB94-1002 and the Human Capital and Mobility Program (Network on Magnetic Molecular Materials from EECC) through Grant ERBCHRXCT920080 are gratefully acknowledged. R.R. and B.C. thank the Ministerio de Educación y Ciencia (Spain) and the Conselleria de Educació i Ciència de la Generalitat Valènciana (Spain) for post- and predoctoral grants, respectively.

Supporting Information Available: Tables of ^{1}H NMR and analytical data for the oxamide ligands and the copper(II) monomeric complexes (Table S1 and S2, respectively) and figures showing the simulation of the EXAFS data and modulus of the Fourier transform for compound **3** using the parameters extracted from the FEFF calculation (Figure S1), the Fourier transforms of the FEFF calculation on the model compound with and without heavy neighbors (Figure S2), the stereoscopic view of the theoretical three-dimensional structure for **1**−**3** (Figure S3), and the χT versus T plot for compounds **1** and **2** (Figures S4 and S5, respectively) (3 pages). Ordering information is given on any current masthead page.

CM9602961

(34) Turner, S. S.; Michaut, C.; Kahn, O.; Ouahab, L.; Lecas, A.; Amouyal, E. *New J. Chem.* **1995**, *19*, 773.

(35) $(NBu_4)_2Mn_2[Cu(Pn_2opbox)]_3 \cdot 4H_2O$ have been also synthesized, where $[NBu_4]^+$ is the tetra-*n*-butylammonium cation and Pn_2opbox stands for *o*-phenylenebis(*N*′-pentyloxamidate). This compound shows characteristic ferrimagnetic behavior with a minimum in the χT versus T plot around 120 K like compounds **1**−**3** and an abrupt ferromagnetic phase transition below a critical temperature T_c = 14 K. Unpublished result.

(36) Okawa, H.; Mitsumi, M.; Ohba, M.; Kodera, M.; Matsumoto, N. *Bull. Chem. Soc. Jpn.* **1994**, *67*, 2139.

(37) Lindsey, J. S. *New J. Chem.* **1991**, *15*, 153 and references therein.

(38) Lehninger, A. L. *Biochemistry*; Worth Publishers: New York, 1975.